Molecular Simulation Study on the Influence of the Scratching Velocity on Nanoscopic Contact Processes

Sebastian Schmitt
Laboratory of Engineering Thermodynamics (LTD), TU Kaiserslautern, Germany

Simon Stephan[1]
Laboratory of Engineering Thermodynamics (LTD), TU Kaiserslautern, Germany

Benjamin Kirsch
Institute for Manufacturing Technology and Production Systems (FBK), TU Kaiserslautern, Germany

Jan C. Aurich
Institute for Manufacturing Technology and Production Systems (FBK), TU Kaiserslautern, Germany

Eberhard Kerscher
Materials Testing (AWP), TU Kaiserslautern, Germany

Herbert M. Urbassek
Physics Department and Research Center OPTIMAS, TU Kaiserslautern, Germany

Hans Hasse
Laboratory of Engineering Thermodynamics (LTD), TU Kaiserslautern, Germany

Abstract

The influence of the scratching velocity on mechanical and thermal properties of a nanoscopic contact process was studied by molecular dynamics simulations. Simulations with different scratching velocities were conducted in dry and lubricated systems. The contact process consisted of a lateral scratching of a spherical indenter on a planar substrate. All molecular interactions were described by the Lennard-Jones truncated and shifted potential. The forces on the indenter, the coefficient of friction and the work done by the indenter as well as the power applied on the indenter were sampled. Furthermore, an analysis of thermal properties was conducted: The change of the energy of the substrate, the indenter and the fluid was evaluated and the local temperature field was determined. The forces, the coefficient of friction and the work done by the indenter show practically no influence of the scratching velocity. The work done by the indenter was found to be the same for all velocities. As a consequence, the power supplied to the system depends linearly on the scratching velocity, which affects the temperature of the contact zone. As expected, the presence of a lubricant reduces the temperature of the substrate in the vicinity of the contact.

2012 ACM Subject Classification Applied computing → Physical sciences and engineering

Keywords and phrases Nanotribology, Friction, Scratching, Lubrication, Lennard-Jones Potential

Digital Object Identifier 10.4230/OASIcs.iPMVM.2020.17

Funding The authors gratefully acknowledge financial support by the Deutsche Forschungsgemeinschaft (DFG, German Research Foundation) – 252408385 – IRTG 2057.

Acknowledgements The present work was conducted under the auspices of the Boltzmann-Zuse Society of Computational Molecular Engineering (BZS). The simulations were carried out on the Regional University Computing Center Kaiserslautern (RHRK) under the grant TUK-MTD, the High Performance Computing Center Stuttgart (HLRS) under the grant MMHBF2 as well as the Leibniz Supercomputing Centre (LRZ) under the grant (AMSEL)ˆ2 (pn56mo).

[1] Corresponding author

© Sebastian Schmitt, Simon Stephan, Benjamin Kirsch, Jan C. Aurich, Eberhard Kerscher, Herbert M. Urbassek, and Hans Hasse;
licensed under Creative Commons License CC-BY 4.0

2nd International Conference of the DFG International Research Training Group 2057 – Physical Modeling for Virtual Manufacturing (iPMVM 2020).
Editors: Christoph Garth, Jan C. Aurich, Barbara Linke, Ralf Müller, Bahram Ravani, Gunther Weber, and Benjamin Kirsch; Article No. 17; pp. 17:1–17:16

OpenAccess Series in Informatics
OASICS Schloss Dagstuhl – Leibniz-Zentrum für Informatik, Dagstuhl Publishing, Germany

1 Introduction

Contact processes play an important role in different fields of technology, e.g. during machining processes between the cutting tool and the workpiece and in bearings between roughness asperities of two macroscopic surfaces. Because of the small dimensions of the actual contact zone, the processes therein can barely be investigated experimentally and, therefore, molecular dynamics (MD) simulations are usually used to investigate nanoscopic contacts [42]. In molecular dynamics simulations, Newton's equations of motion are solved for an atomistic many-particle system. The interactions of the particles in molecular dynamics simulations are often described by classical force fields. Molecular dynamics simulations are known to have good predictive capabilities and are widely used to simulate material properties [23, 39, 41] as well as nanoscale processes [15]. In molecular simulations of contact processes, the macroscopic contact is usually reduced to a single surface asperity in contact with a flat surface [13]. The actual contact process is usually modeled by a sequential movement of the indenter: (1) The indenter is brought into contact with the substrate during the indentation phase; (2) the indenter carries out a lateral scratching through the substrate surface during the scratching phase. The present work studies the influence of the indenter velocity during the scratching.

There are many studies focusing on different aspects of dry nanoscratching. They address the influence of the indenter geometry [2], different substrate materials [1, 49], the surface orientation [16] and dislocations [18]. There are few studies available in the literature addressing the comparison of lubricated and dry nanoscratching processes [27,28,34,35,38,40]; most studies on nanoscopic contact processes do not consider the presence of a fluid as lubricant and cooling agent [45]. The influence of the lubricant on both mechanical and thermal properties like the coefficient of friction or the temperature field were studied in the present work at different scratching velocities.

The influence of the scratching velocity in nanoscopic scratching processes was subject of several studies [19, 29, 31, 32, 47, 48, 50], however, mostly for dry contacts. Only Ren et al. [34] investigated the influence of the scratching velocity on mechanical properties (the forces on the indenter and the coefficient of friction) in a system with a thin water film as lubricant. Overall, scratching velocities in the range of 1 – 400 m/s were applied [34, 48]. The influence of the scratching velocity on different mechanical properties were investigated, whereas little is known on the influence on thermal properties. Only the influence of the scratching velocity on the temperature of the substrate has been studied [29, 31]. Most authors report a decrease of the coefficient of friction with increasing scratching velocity in the dry case [32, 50]. As expected, the temperature in the contact zone increases with increasing scratching velocity [19, 48]. For lubricated systems, Ren et al. [34] found that the coefficient of friction does not depend on the scratching velocity. Besides the influence of the velocity in a scratching process, the influence of the velocity on a process of indentation has been studied more thoroughly, e.g. Refs. [3, 17, 36].

Most molecular simulation studies on contact processes investigate mechanical properties focusing on the impact on the substrate, e.g. elastic and plastic deformation, the dislocation behavior, the friction forces and the coefficient of friction [18, 49]. Thermal properties such as the temperature field in the contact zone or the energy balance of the process have been investigated only by few authors [35, 38]. The energy balance of the process is of particular interest in the lubricated case to evaluate the cooling capability of the fluid, which is of fundamental importance in tribological and machining applications [7, 24, 30].

In the present study, molecular dynamics simulations of a generalized model system were used to study the influence of the scratching velocity on both mechanical and thermal properties. Both dry and lubricated cases were considered. By systematically investigating

the influence of the scratching velocity on both dry and lubricated contact processes, this study stands out from previous studies in the literature. The lateral scratching movement of a spherical indenter on a planar surface was analysed in detail. All occurring interactions were modeled with the Lennard-Jones truncated and shifted (LJTS) potential. The LJTS potential is frequently used in the literature [12, 21, 26] as it is computationally particularly cheap and can describe the properties of small, spherical molecules well [46]. The studied scratching velocities are in the range of 20 m/s – 100 m/s, which are typical conditions in grinding processes in manufacturing applications [25]. Within this range, five different velocities were chosen and applied in both the dry and the lubricated case.

2 Methods

2.1 Molecular Model

The simulation scenario includes three different substances: The solid substrate, the spherical solid indenter and the fluid (cf. Fig. 1). The latter is only present in the lubricated cases.

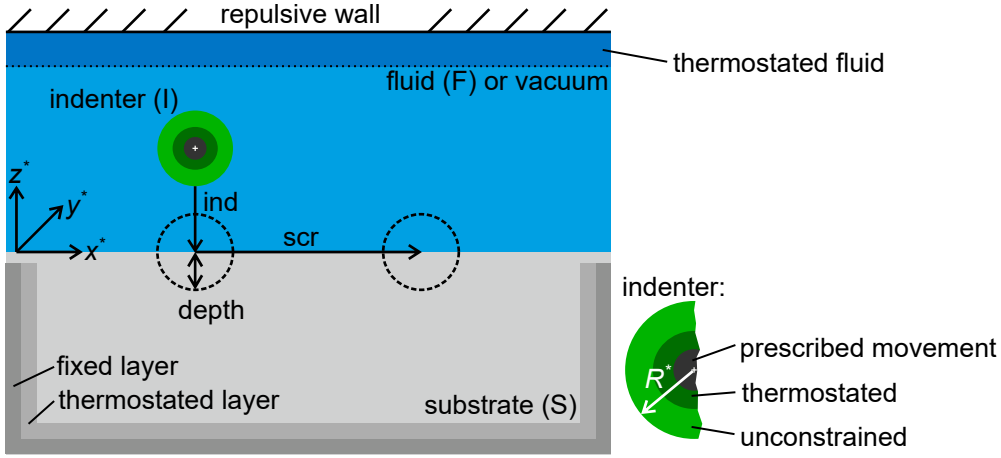

Figure 1 Simulation scenario (not true to scale) with substrate (grey), indenter (green) and vacuum (dry cases, blue) or fluid (lubricated cases, blue). Simulation procedure: First indentation (ind) of indenter, then scratching (scr).

All occurring intermolecular interactions are modeled with the LJTS potential

$$U_{\mathrm{LJTS}}(r) = \begin{cases} U_{\mathrm{LJ}}(r) - U_{\mathrm{LJ}}(r_{\mathrm{c}}) & r \leq r_{\mathrm{c}} \\ 0 & r > r_{\mathrm{c}} \end{cases} \quad \text{with} \quad U_{\mathrm{LJ}}(r) = 4\,\varepsilon \left[(\sigma/r)^{12} - (\sigma/r)^{6} \right], \tag{1}$$

where σ is the size parameter, ε the energy parameter and r the distance between two particles. The full Lennard-Jones potential is denoted by $U_{\mathrm{LJ}}(r)$. The cut-off radius is $r_{\mathrm{c}} = 2.5\,\sigma$ for all site-site interactions except the solid-solid interaction between the substrate and the indenter particles. For the solid-solid interaction the cut-off radius is chosen as $r_{\mathrm{c}} = 2^{1/6}\,\sigma$ such that the indenter-substrate interactions are purely repulsive (the potential is truncated at the potential minimum). All occurring physical quantities in this work are reduced using the parameters of the potential of the fluid particles σ_{F}, ε_{F} and the mass of a fluid particle m_{F} [4] using the relations given in Table 1. The size parameter σ of the potentials of all three substances as well as the masses m of all particles were equal.

Table 1 Definition of physical quantities in reduced units. The asterisk (*) indicates a reduced quantity. k_B is the Boltzmann constant.

Length	$L^* =$	L/σ_F
Temperature	$T^* =$	$T/(\varepsilon_\mathrm{F}/k_\mathrm{B})$
Force	$F^* =$	$F/(\varepsilon_\mathrm{F}/\sigma_\mathrm{F})$
Time	$t^* =$	$t/(\sigma_\mathrm{F}\sqrt{m_\mathrm{F}/\varepsilon_\mathrm{F}})$
Velocity	$v^* =$	$v/\sqrt{\varepsilon_\mathrm{F}/m_\mathrm{F}}$
Energy	$E^* =$	E/ε_F
Power	$P^* =$	$P/\sigma_\mathrm{F}\sqrt{m_\mathrm{F}/\varepsilon_\mathrm{F}^3}$

Table 2 shows the energy parameters for the interactions between particles of the substrate, the indenter and the fluid. Both interactions with particles from the same substance (diagonal elements) and with particles from another substance (off-diagonal elements) are included in Table 2. The energy parameter for the fluid ε_F was chosen such that it models the thermodynamic properties of methane [46]. The energy parameter of the substrate particles ε_S was adopted from Ref. [20] such as to represent iron. The energy parameter for the indenter ε_I was chosen sufficiently large such that no plastic deformations or dislocations occur in the indenter and that there is no wear of the indenter in the process (this was tested in preliminary simulations). The chosen solid-fluid interaction energy between the fluid and the substrate particles $\varepsilon_\mathrm{S\text{-}F}$ as well as between the fluid and the indenter particles $\varepsilon_\mathrm{I\text{-}F}$ was chosen to be in the domain of total wetting [5]. All simulations were carried out using LAMMPS [33].

Table 2 Pairwise interaction energy parameters used in the simulations. The size parameter σ of all potentials and the molar mass M of all particles were $\sigma = 3.7241$ Å [46] and $M = 16.043$ g/mol, respectively.

	Substrate	Indenter	Fluid
Substrate	$\varepsilon^*_\mathrm{S} = 34.89$	$\varepsilon^*_\mathrm{S\text{-}I} = 300$	$\varepsilon^*_\mathrm{S\text{-}F} = 1.5$
Indenter		$\varepsilon^*_\mathrm{I} = 200$	$\varepsilon^*_\mathrm{I\text{-}F} = 1.5$
Fluid			$\varepsilon_\mathrm{F} = 175.06$ K/k$_\mathrm{B}$

2.2 Simulation Setup

The dimension of the simulation box in x^*, y^* and z^*-direction was $L^*_\mathrm{x} = 241.30$, $L^*_\mathrm{y} = 120.64$ and $L^*_\mathrm{z} = 194.81$. In x^* and y^*-direction, periodic boundary conditions were applied. At the top, the simulation box was enclosed by a soft repulsive wall with a harmonic potential. The substrate block comprised the whole x^*-y^* plane and had a height of $\Delta z^* = 116.56$. The principles of the simulation setup were adopted from Ref. [40]. The simulation procedure was as follows: In a first step, the initial density of the fluid ($\rho^* = 0.804$, which is a liquid state at the given temperature) was adjusted (only in the lubricated cases) by moving the upper repulsive wall in negative z^*-direction. Subsequently, the entire simulation box was equilibrated at the initial temperature $T^* = 0.8$. The equilibration was carried out for 5×10^5 time steps. The time step was $\Delta t^* = 0.0008$ in all simulations. After the equilibration, the indentation started by moving the indenter in negative z^*-direction until the depth of penetration $z^* = -6$ was reached (cf. Fig. 1). Two different simulation setups were

considered in the present work: Dry cases and lubricated cases. To study the influence of the scratching velocity, two base simulations were equilibrated and indented: One dry and one lubricated. These two equilibrated setups were used in several scratching simulations. Hence, the initial conditions for each of the dry and lubricated cases, respectively, were identical at the beginning of the scratching process. The indenter scratched in lateral, i.e. positive x^*-direction, for a total length of $L^*_{\mathrm{max}} = 80.56$ in all simulations. Five different scratching velocities $v^*_{\mathrm{scr}} = 0.066, 0.133, 0.204, 0.266$ and 0.332 were studied – each for the dry and the lubricated cases. These scratching velocities correspond to 20, 40, 60, 80 and 100 m/s (using the potential parameters of Table 2).

The origin of the Cartesian coordinate system was defined such that $z^* = 0$ was the height of the initial undeformed surface of the substrate and $x^* = 0$ and $y^* = 0$ were located in the corner of the simulation box. The substrate consisted of 3.65×10^6 particles arranged on a single crystal face cubic centered (fcc) lattice, which is the equilibrium lattice at the given state [37, 43]. The surface orientation was (100). The scratching was conducted in [1 1 0] surface direction. To fix the substrate block in place, layers with fixed atom positions were employed at the simulation box boundaries. To model the heating of the surrounding material, thermostated layers were located between the actual substrate and the fixed layers (cf. Fig. 1).

The spherical indenter had a radius of $R^* = 12.08$ and, similar to the substrate, consisted of three parts. For particles in the core ($R^* \leq 2.69$), the motion was prescribed to realize the relative motion of the indenter with respect to the substrate. Around the core, there was a thermostated shell with a thickness of $\Delta R^* = 2.69$. The particles of the outer shell ($R^* > 5.38$) were unconstrained and moved freely following Newton's equations of motion. The thickness of the thermostated layer was chosen such that the particles of the outer shell did not interact with the rigid core. The indenter consisted of 7935 particles which were, as the substrate, arranged on an fcc lattice.

In the lubricated cases, the indenter was fully immersed in the fluid, which consisted of 1.78×10^6 particles. A fluid region at the top of the simulation box below the soft repulsive wall ($62.14 < z^* < 78.25$) was thermostated. The thermostating in all three thermostated zones (substrate, indenter and fluid) was carried out using the Berendsen thermostat [6] to constrain their temperature constant at $T^* = 0.8$. The thermostated layers removed the dissipated thermal energy from the simulation box.

2.3 Definition of Observables

To examine the influence of the scratching velocity on the contact process and to compare the results from the dry and the lubricated cases various mechanical and thermal properties were used. They are defined in the following. The total tangential and normal forces on the indenter F^*_{t} and F^*_{n} were computed as the sum of the forces in x^* and z^*-direction acting on all indenter particles, respectively. From the forces on the indenter, the coefficient of friction was calculated from $\mu = -F^*_{\mathrm{t}}/F^*_{\mathrm{n}}$. The work done by the indenter was calculated from $W^*_{\mathrm{I}} = \int -F^*_{\mathrm{t}} \mathrm{d}x^*$. The power supplied to the system was calculated from $P^*_{\mathrm{I}} = \mathrm{d}W^*_{\mathrm{I}}/\mathrm{d}t^*$.

Furthermore, the change of the energy ΔE^*_j in the three parts of the simulation box was calculated as: $\Delta E^*_j = \Delta U^*_j + \Delta E^*_{\mathrm{thermo},j}$ for j = S, I, F (substrate, indenter and fluid). The change of the energy ΔE^*_j is composed of the change of the internal energy ΔU^*_j (sum of kinetic and potential energy) of the respective part and the energy removed by the respective thermostat $\Delta E^*_{\mathrm{thermo},j}$. The change of the internal energy ΔU^*_j includes the change of the kinetic energy of the respective parts as well as the energy of the elastic and the plastic deformation (only for the solids), which is part of the potential energy. For simplicity, all these

contributions are summarized in the single observable ΔE_j^* although this reflects different phenomena of the process such as the dissipation of the work done on the system, elastic and plastic deformation of the solids and the heat flow to the surroundings as represented by the action of the thermostats in the thermostated zones. The corresponding change of the energy per time $\mathrm{d}E_j^*/\mathrm{d}t^*$ is defined as the derivative of the change of the energy with respect to time.

To characterize the thermodynamic behavior of the system, the temperature in the contact zone T^*_{contact} was evaluated as the mean temperature of the substrate particles in a volume V^*_{contact} in front of the indenter (cf. Fig. 2), whereas the directed velocity from the particles is subtracted from the total average kinetic energy for the computation of the local temperature by the thermal motion, cf. Ref. [38] for details. The contact volume V^*_{contact} has the dimensions $2\,R^* \times 2\,R^* \times 3\,R^*$, where R^* is the radius of the indenter. Furthermore, the temperature distribution in the x^*-z^* plane was sampled during the simulations: A stripe at $y^* = L^*_{\mathrm{y}}/2$ with an extend of $\Delta y^* = 2.15$ was segmented into cuboid bins (with $\Delta x^* = \Delta z^* = 1.34$), in which the temperature was averaged over 5000 time steps in every bin (cf. Fig. 2). The gap between the indenter and the substrate was defined as the space between the two bodies below the undeformed surface level and in front of the center of the indenter. This lubrication gap definition is used to count the fluid particles trapped between the two solid bodies, cf. Fig. 2.

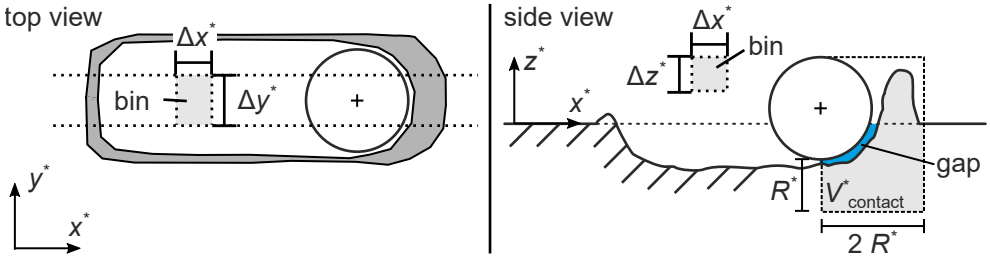

Figure 2 Scheme for illustrating the observables and bins to spatially evaluate the temperature. Left (top view): Definition of the bins in the x^*-y^* plane with $\Delta x^* = 1.34$ and $\Delta y^* = 2.15$. Right (side view): Definition of the gap between the indenter and the substrate (blue), the volume V^*_{contact} (light grey) and the bins in the x^*-z^* plane with $\Delta x^* = \Delta z^* = 1.34$.

3 Results and Discussion

3.1 Mechanical Properties

The results for the tangential and normal forces on the indenter F_{t}^* and F_{n}^* as well as the coefficient of friction μ as a function of the scratching length L^*_{scr} are shown in Fig. 3. At the beginning of the scratching ($L^*_{\mathrm{scr}} < 5$), the tangential force F_{t}^* in the dry and the lubricated cases shows a steep decrease. During the ongoing scratching process, the tangential force fluctuates in the range $-4 < F_{\mathrm{t}}^*/10^3 < -2$ in the dry and the lubricated cases. As expected, the value of the tangential force is negative such that it acts as a force against the direction of motion. No significant differences between the results for the dry and lubricated cases are observed. The scratching velocity has no significant influence on the forces of the contact process in the studied range of scratching velocities.

The normal force F_{n}^* in the dry cases is approximately 6.5 at the beginning of the scratching and decreases within $L^*_{\mathrm{scr}} < 10$ to values in the range $2 < F_{\mathrm{n}}^*/10^3 < 5$. The normal force in the lubricated cases has a similar behavior. The values of F_{n}^* after the indentation ($L^*_{\mathrm{scr}} = 0$) are higher in the lubricated cases due to fluid particles confined

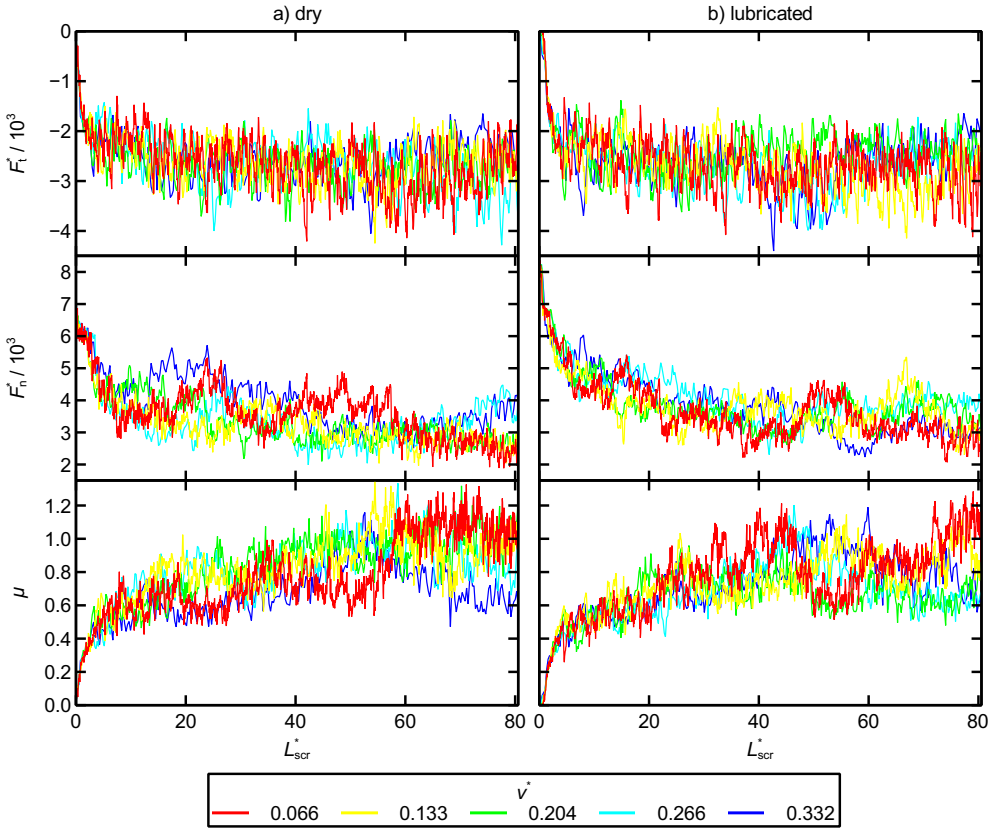

Figure 3 Tangential force F_t^* (top), normal force F_n^* (middle) on the indenter and coefficient of friction μ (bottom). Results of simulations for dry cases (left) and lubricated cases (right) from all five considered scratching velocities as function of the scratching length L_{scr}^*.

between the indenter and the substrate, cf. Ref. [40] for a detailed discussion. Additionally, the decrease of the normal force F_n^* is less steep in the lubricated cases and only reaches a constant level for $L_{scr}^* > 20$, where the values are in the range of $2 < F_n^*/10^3 < 5$ like in the dry cases. The difference of the decrease of F_n^* in the lubricated cases is due to the presence of fluid particles in the gap between the substrate and the indenter. These fluid particles are squeezed out during the starting phase of the scratching [40]. The normal force on the indenter exhibits stronger fluctuations compared to the tangential force during the scratching.

The coefficient of friction μ was calculated from the tangential and normal force and therefore shows similar characteristics. In the dry cases, the coefficient of friction μ increases within $L_{scr}^* < 10$ up to $\mu \approx 0.6$ and then fluctuates in a range between 0.5 and 1.2. The differences between the individual simulations build up to a scratching length of $L_{scr}^* = 80$. As already observed for the normal force, the starting phase in which the coefficient of friction increases from $\mu = 0$ at $L_{scr}^* = 0$ is longer in the lubricated cases. Up to a scratching length of $L_{scr}^* \approx 20$, the coefficient of friction increases and fluctuates in the range $0.5 < \mu < 1.2$ for $L_{scr}^* > 20$.

For a better comparison, the simulation data were averaged in the quasi steady state regime. This regime is defined as $L_{scr}^* > 20$. It has been shown that the number of fluid particles in the gap between the indenter and the substrate is practically constant in this

steady state regime [40]. Fig. 4 shows the number of fluid particles in the gap between the indenter and the substrate. Starting at the beginning of the scratching, the fluid particles are squeezed out of the gap. At the beginning of the scratching, there are around 90 particles in the gap that are rapidly squeezed out of the gap with ongoing lateral movement. In the simulations with higher scratching velocity, there is a tendency that the particles are squeezed out slightly faster – especially from $L^*_{\mathrm{scr}} = 10$ up to $L^*_{\mathrm{scr}} = 40$. Until $L^*_{\mathrm{scr}} = 20$, the number of particles remaining in the gap is reduced to less than 20 particles in all simulations. These few isolated atoms are scattered in the contact zone. Consequently, the actual contact zone is mainly dry and there is no fluid flow in the contact zone. For $L^*_{\mathrm{scr}} > 20$, the number of particles in the gap remains approximately constant. This establishes the steady state regime. The results for the friction forces and the coefficient of friction (cf. Fig. 3) corroborate this classification.

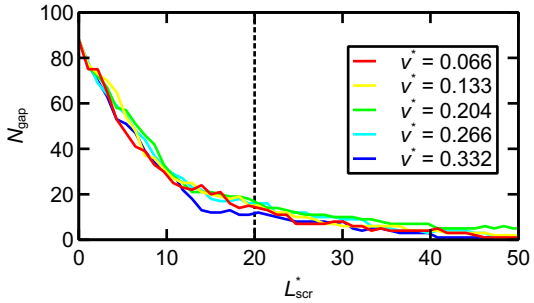

Figure 4 Number of fluid particles in the gap N_{gap} between substrate and indenter as function of scratching length L^*_{scr} in the lubricated cases (cf. Fig. 2).

Fig. 5 shows the mean coefficient of friction μ as a function of the scratching velocity v^* averaged in the steady state regime. No distinct dependency of the coefficient of friction on the scratching velocity is found in the considered velocity range. For a scratching velocity $v^* = 0.066$ the coefficients of friction in the lubricated and the dry case are almost equal and lie around $\mu \approx 0.85$. Nearly equal values for the coefficient of friction at this velocity have also been observed in a previous work of our group [38] with a similar simulation scenario. Therein, a cylindrical indenter with a slightly smaller indenter radius was used. Furthermore, for the simulations reported in Ref. [38] no thermostats were applied in the indenter and the fluid. For the higher scratching velocities, the coefficient of friction in the dry and the lubricated cases remains nearly constant, but scatters intensely. The values fluctuate in the range $0.7 < \mu < 0.9$ for the dry and the lubricated cases. For moderate scratching velocities ($0.1 < v^* < 0.3$), the lubricated cases yield a slightly lower coefficient of friction. Nevertheless, these differences are probably within the uncertainty of the data. Noreyan and Amar [32] and Zhu et al. [50] have performed dry scratching simulations at different scratching velocities and found a decrease of the coefficient of friction by at least 25 % with increasing scratching velocity in the range $v^* = 0.16$ – $v^* = 1.42$. This decrease was reported [32, 50] to be more pronounced at high scratching velocities, i.e. $v^* > 0.332$ (which corresponds to approximately $v > 100$ m/s). However, it should be noted that the simulation scenarios from Refs. [32, 50] and from this work differ regarding the indenter shape and the molecular force fields which is known to influence the coefficient of friction [2]. For indentation processes, it has been found that the effect of the indenter velocity on the simulation results is small as long as it is below around 100 m/s [3, 17, 36]. The reason hereto is that the plastic deformation processes in the sample are based on dislocation generation, which are only little affected by the indenter

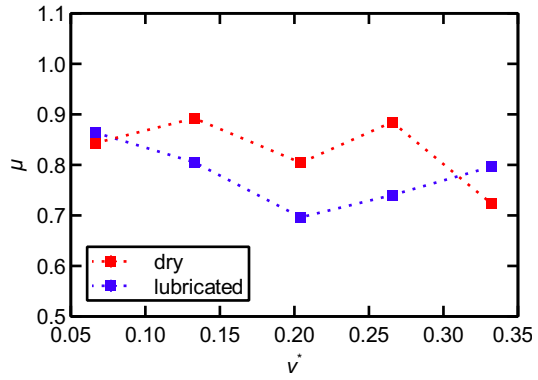

Figure 5 Mean coefficient of friction μ as function of the scratching velocity v^* for the dry and the lubricated cases. Lines are a guide to the eye.

velocity in the regime of around 0.01 – 100 m/s. At smaller indenter velocities, however, thermal effects may influence dislocation generation, reaction and migration, while at higher velocities, the sample starts to amorphize locally.

Fig. 6 shows the work done by the indenter W_I^* as function of the scratching velocity v^*. All values lie in the range $2.1 < W_\mathrm{I}^*/10^6 < 2.4$. For both the dry and the lubricated case,

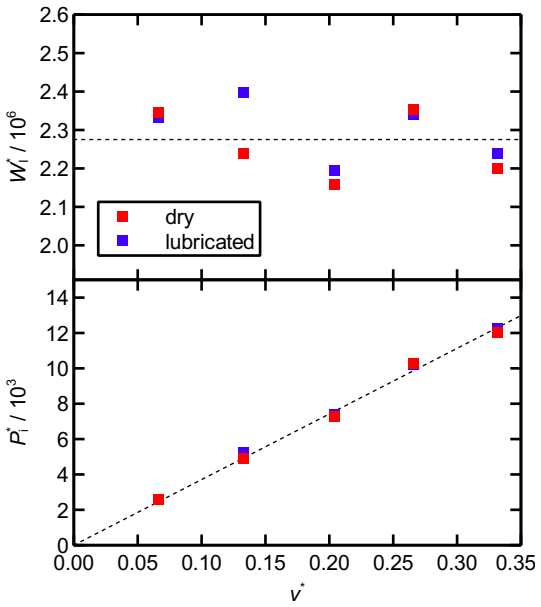

Figure 6 Work done by the indenter W_I^* (top) and power supplied to the system by the indenter P_I^* in the steady state regime as function of the scratching velocity v^* for the dry and the lubricated cases. The dotted lines indicate the average of the work done by the indenter $\overline{W_\mathrm{I}^*} = 2.28 \times 10^6$ (top) of all simulations and a linear function (bottom) $P_\mathrm{I}^* = a \cdot v^*$ fitted to the data of the dry simulations ($a = 37.1 \times 10^3$).

no dependency on the scratching velocity is observed as expected from the results for the tangential force (cf. Fig. 3). The power P_I^* supplied to the system by the indenter motion is also shown in Fig. 6. The power P_I^* in both the dry and the lubricated case is linearly dependent on the scratching velocity v^* as expected from the nearly constant work done

by the indenter shown in Fig. 6 and the shortening of the simulation time with increasing scratching velocity. The values of the power reach from $P_{\mathrm{I}}^{*} = 2.6 \times 10^{3}$ at $v^{*} = 0.066$ to $P_{\mathrm{I}}^{*} = 12.2 \times 10^{3}$ at $v^{*} = 0.332$. No significant differences between the dry and the lubricated cases are observed. The dotted line shown in Fig. 6 represents the linear function $P_{\mathrm{I}}^{*} = 37.1 \times 10^{3} \cdot v^{*}$ that was fitted to the results of the dry cases. The form of the function was chosen such that it reflects the limit $P_{\mathrm{I}}^{*} = 0$ for $v^{*} \to 0$. For $v^{*} \to 0$, the scratching time becomes infinite and the power goes to zero.

3.2 Thermal Properties

Besides the mechanical properties, also thermal properties of a contact process play an important role in technical applications. First, the change of the energy ΔE_{j}^{*} in the three parts of the simulation (substrate, indenter and fluid) are shown in Fig. 7 for the steady state regime ($L_{\mathrm{scr}}^{*} > 20$). The sampled changes of the energies are found to be independent of the scratching velocity. The work done by the indenter is portioned into a change of the energy of the substrate, of the fluid and of the indenter. The largest portion of the energy supplied to the system by the indenter goes into the substrate with about $\overline{\Delta E_{\mathrm{S}}^{*}} = 2.1 \times 10^{6}$ in the dry cases and $\overline{\Delta E_{\mathrm{S}}^{*}} = 1.94 \times 10^{6}$ in the lubricated cases. The increase of the energy of the indenter $\Delta E_{\mathrm{I}}^{*}$ are much smaller than the increase of the energy of the substrate $\Delta E_{\mathrm{S}}^{*}$ and are around $0.08 < \Delta E_{\mathrm{I}}^{*}/10^{6} < 0.16$. The change of the energy of the fluid $\Delta E_{\mathrm{F}}^{*}$ is about twice the change of the energy of the indenter $\Delta E_{\mathrm{I}}^{*}$ in the lubricated cases and lies in the range $0.2 < \Delta E_{\mathrm{F}}^{*}/10^{6} < 0.25$. The energy increase of the substrate and the indenter is significantly reduced in the lubricated cases compared to the dry ones. This reduction is simply due to the fact that a significant portion of the work done by the indenter goes into the fluid – if such is present. The reduction of the energy increase of the substrate and the indenter is fairly independent of the scratching velocity.

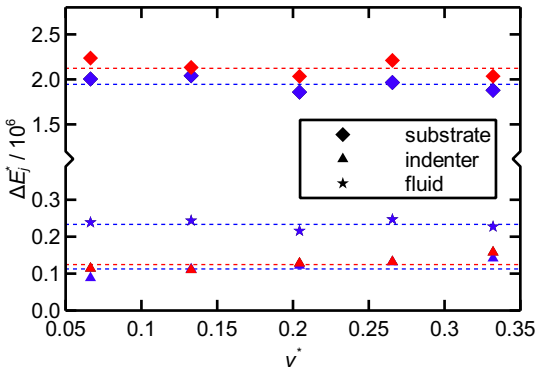

Figure 7 Change of the energy in the substrate $\Delta E_{\mathrm{S}}^{*}$, the indenter $\Delta E_{\mathrm{I}}^{*}$ and the fluid $\Delta E_{\mathrm{F}}^{*}$ in the steady state regime ($L_{\mathrm{scr}}^{*} > 20$) as function of the scratching velocity v^{*} in the dry (red) and the lubricated (blue) cases. The dotted lines represent the mean over all scratching velocities of the respective data (dry: $\overline{\Delta E_{\mathrm{S}}^{*}} = 2.12 \times 10^{6}$, $\overline{\Delta E_{\mathrm{I}}^{*}} = 0.12 \times 10^{6}$; lubricated: $\overline{\Delta E_{\mathrm{S}}^{*}} = 1.94 \times 10^{6}$, $\overline{\Delta E_{\mathrm{I}}^{*}} = 0.11 \times 10^{6}$, $\overline{\Delta E_{\mathrm{F}}^{*}} = 0.23 \times 10^{6}$).

To evaluate the energy balance in more detail, we compare the sum of the means over all scratching velocities of the changes of the energy to the work done by the indenter using the following equation: $\overline{W_{\mathrm{I}}^{*}} = \overline{\Delta E_{\mathrm{S}}^{*}} + \overline{\Delta E_{\mathrm{I}}^{*}} + \overline{\Delta E_{\mathrm{F}}^{*}} + \delta$. Here, δ represents the numerical error which arises from rounding errors as well as the error occurring during numerical integration. The error is less than 1 % in all simulations. The energy balance reveals that in the dry

cases around 94.2 % of the work done by the indenter causes an increase of the energy of the substrate. The remainder of the work done by the indenter leads to an increase of the energy of the indenter. In the lubricated cases, 10 % of the work done by the indenter causes an increase of the energy of the fluid. Therefore, less energy goes into the substrate (about 84 %) and into the indenter (only about 5 %). These values are similar to results obtained in a previous work of our group [38]. Comparing the dry and the lubricated cases, the energy increase of the substrate ΔE^*_S is reduced by 8.5 % and the energy increase ΔE^*_I of the indenter is reduced by 9.5 %. This is due to the increase of the energy of the fluid ΔE^*_F and leads to the expected cooling effect for both the substrate and the indenter.

The results obtained from the simulations with different scratching velocities for the change of the energy per time $\mathrm{d}E^*_j/\mathrm{d}t^*$ in the steady state regime ($L^*_\mathrm{scr} > 20$) are shown in Fig. 8. The numbers obtained from $\mathrm{d}E^*_j/\mathrm{d}t^*$ for the substrate, the fluid and the indenter show a linear dependency on the scratching velocity. This is expected as the power supplied to the system also increases linearly with increasing scratching velocity. As expected from the changes of the energy ΔE^*_j shown in Fig. 7, the values $\mathrm{d}E^*_j/\mathrm{d}t^*$ of the substrate ($j = \mathrm{S}$) are highest for all simulations (cf. Fig. 8). This is probably due to the fact that the main part of the work done by the indenter dissipates in the substrate in the vicinity of the contact as a consequence of elastic and plastic deformation.

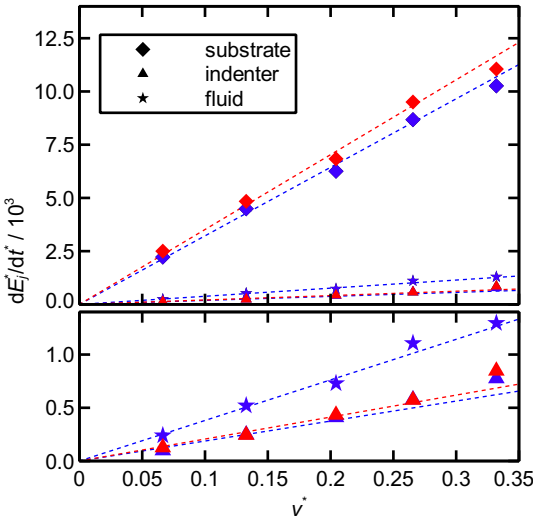

Figure 8 Change of the energy per time in the substrate $\mathrm{d}E^*_\mathrm{S}/\mathrm{d}t^*$, the indenter $\mathrm{d}E^*_\mathrm{I}/\mathrm{d}t^*$ and the fluid $\mathrm{d}E^*_\mathrm{F}/\mathrm{d}t^*$ as function of the scratching velocity v^* in the dry (red) and the lubricated (blue) cases. The dotted lines represent linear functions of the form $\mathrm{d}E^*_j/\mathrm{d}t^* = a \cdot v^*$ fitted to the respective data (dry: $a_\mathrm{S}/10^3 = 35.2$, $a_\mathrm{I}/10^3 = 2.1$; lubricated: $a_\mathrm{S}/10^3 = 32.2$, $a_\mathrm{I}/10^3 = 1.9$, $a_\mathrm{F}/10^3 = 3.8$).

Fig. 9 shows the temperature of the contact zone of the substrate as a function of the scratching velocity. The contact zone temperature was averaged both spatially (cf. Fig. 2) and over time; during the steady state regime. The results of the simulations with a scratching velocity of $v^* = 0.066$ show that the contact zone temperature ($T^*_\mathrm{contact} \approx 0.85$) is slightly increased compared to the initial temperature of $T^* = 0.8$, which was also applied to the thermostats during the contact process. With increasing scratching velocity, the contact zone temperature increases linearly. This is a consequence of the dependency of the change of the energy per time on the scratching velocity, cf. Fig. 8. The contact zone temperature can be described by a linear function which assumes no temperature change of the contact zone

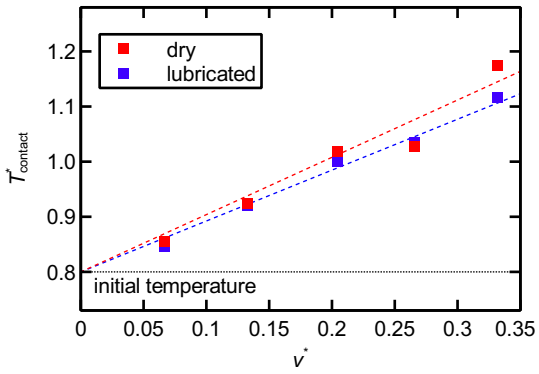

Figure 9 Temperature of the substrate in the contact zone T^*_{contact} (cf. Fig. 2) as function of the scratching velocity v^* in the dry and the lubricated cases averaged in the steady state regime ($L^*_{\mathrm{scr}} > 20$). The black dotted line indicates the preset temperature of the thermostats. The red and blue dotted lines represent linear functions $T^*_{\mathrm{contact}} = a \cdot v^* + 0.8$ fitted to the respective data (dry: $a = 1.04$; lubricated: $a = 0.92$).

in the limit $v^* \to 0$. For most scratching velocities, the contact zone temperature is higher in the dry cases than in the corresponding lubricated cases (except the scratching velocity of $v^* = 0.266$). This effect is due to the presence of the fluid since a part of the work done by the indenter goes into the fluid (cf. Fig. 8), which confirms the findings from Ref. [38]. The cooling of the substrate in the contact zone is the primary task of the fluid in macroscopic cutting processes [8, 9, 22]. The absolute difference of the contact zone temperature between the dry and the lubricated cases slightly increases with increasing scratching velocity. This is also in accordance to the increase of the change of the energy per time of the fluid with increasing scratching velocity (cf. Fig. 8). The increase of the contact zone temperature with increasing scratching velocity has already been reported by several studies [19, 29, 31, 48, 50] for dry cases. The results from the present study extend this phenomenon to lubricated systems, where the thermal balance is influenced by several additional phenomena at the interface and in the fluid [38].

The spatial temperature distribution is discussed by means of snapshots of the x^*-z^* plane at the scratching length of $L^*_{\mathrm{scr}} = 77$, cf. Fig. 10. The setup of the bins used for the spatial discretization is shown in Fig. 2. Surface lines of the substrate and the indenter are directly extracted from the position data of the particles using an alpha shape algorithm. Details of the applied post-processing algorithm can be found in Ref. [14]. The snapshots are shown for the scratching velocities $v^* = 0.066$, 0.204 and 0.332. For the velocity $v^* = 0.066$, there is a slight increase of the local temperature up to $T^* \approx 0.96$ observed in the tip of the chip in the dry case. In the bulk of the substrate, no significant change of the temperature compared to the initial temperature ($T^* = 0.8$) is found. In the lubricated cases, the increase of the local temperature in the contact zone is reduced by the presence of the fluid (cf. Fig. 10). Increasing the scratching velocity yields an increase of the temperature in the chip in the dry cases (cf. Fig. 10 at $v^* = 0.204$ and 0.332). The maximum local temperature at the velocity of $v^* = 0.332$ is $T^* = 1.77$ and is reached in the chip. Overall the warming of the substrate is mainly limited to the chip and the direct vicinity of the contact zone, which is the most plastically deformed zone of the substrate. The concentration of warming of the substrate in the chip has also been reported by Refs. [11, 28]. For the temperature field of the fluid in the lubricated cases, the temperature is mainly increased in the area around the chip. This indicates that the increase of the internal energy of the fluid mainly takes place by a heat flux from the chip. Therefore, only a small portion of the increase of the internal

energy of the fluid results from actual energy dissipation in the fluid in the contact zone, as practically no fluid is present there. The dissipated energy which increases the internal energy of the fluid during the scratching is hence mainly indirectly transferred to the fluid via the chip and the substrate surface (cf. Fig. 4). The warming of the fluid includes larger spatial dimensions compared to the substrate, which is a direct result of the differences of the thermal conductivity of the substrate, the indenter and the fluid [38]. The fluid has a significantly lower thermal conductivity than the substrate [10, 44].

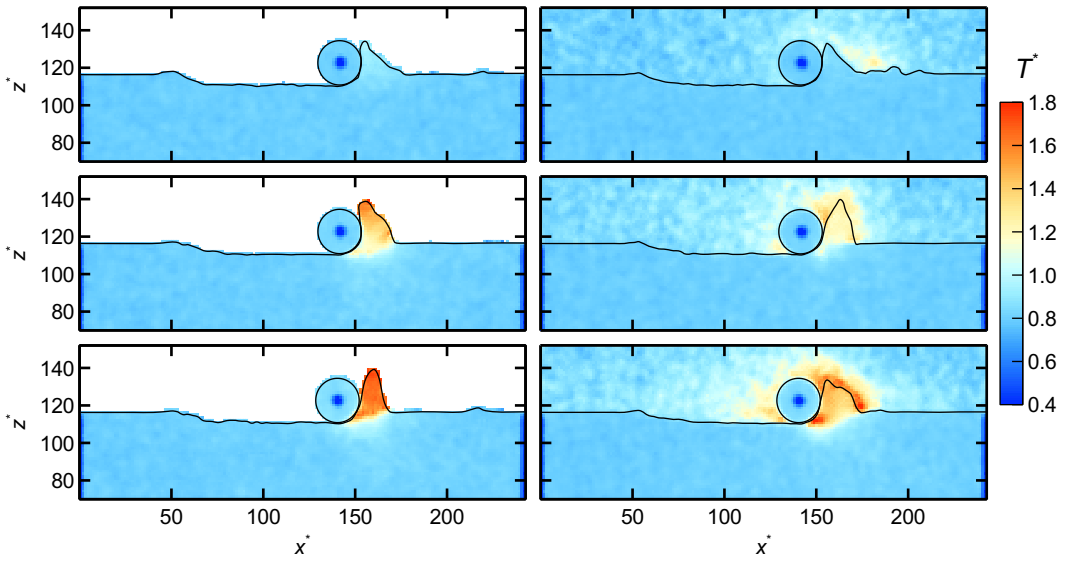

Figure 10 Temperature in x^*-z^* plane for the scratching length $L^*_{\mathrm{scr}} = 77$ for dry (left) and lubricated (right) cases for the scratching velocities $v^* = 0.066$ (top), 0.204 (middle) and 0.332 (bottom). Black lines indicate the surface of the substrate and the indenter.

4 Conclusions

In the present work, the influence of the scratching velocity on dry and lubricated contact processes was studied by molecular dynamics simulations. All intermolecular interactions were modeled by the LJTS potential such that the model is a simplified yet representative system. Mechanical properties like the occurring forces, the coefficient of friction and the power supplied to the system as well as thermal properties like the change of the energy, the energy balance and the local temperature field were evaluated.

The mechanical properties show only a weak dependency on the scratching velocity in the considered velocity range. No significant dependency on the scratching velocity was observed for the coefficient of friction in both dry and lubricated cases. The power supplied to the system by the indenter increases linearly with increasing scratching velocity, which is expected from the shortening of the total scratching time while the total energy supplied to the system remains fairly constant. This independence can be traced back to the plastic deformation processes in the material, which do not change in the velocity regime considered here. The increase of the power supplied to the system by the indenter directly affects the temperature in the contact zone which also shows a linear increase with increasing scratching velocity both in the dry and in the lubricated system. In the lubricated cases, the local temperature in the vicinity of the contact zone is slightly reduced due to the presence of the fluid. The cooling effect of the lubricant is weaker than could have been expected from macroscopic experience. This could indicate that the macroscopic cooling effect of the lubricant is mainly

indirect, i.e. due to a cooling of the substrate and the indenter not in the vicinity of the contact zone but in its surroundings, leading to an increased removal of heat by conduction in the macroscopic system.

References

1 A. T. Al Motasem, J. Bergström, A. Gåård, P. Krakhmalev, and L. J. Holleboom. Atomistic insights on the wear/friction behavior of nanocrystalline ferrite during nanoscratching as revealed by molecular dynamics. *Tribology Letters*, 65(3):101, 2017. doi:10.1007/s11249-017-0876-y.

2 I. Alabd Alhafez, A. Brodyanski, M. Kopnarski, and H. M. Urbassek. Influence of tip geometry on nanoscratching. *Tribology Letters*, 65(1):26, 2017. doi:10.1007/s11249-016-0804-6.

3 J. Alcalá, R. Dalmau, O. Franke, M. Biener, J. Biener, and A. Hodge. Planar defect nucleation and annihilation mechanisms in nanocontact plasticity of metal surfaces. *Physical Review Letters*, 109(7):075502, 2012. doi:10.1103/PhysRevLett.109.075502.

4 M. P. Allen and D. J. Tildesley. *Computer simulation of liquids*. Oxford University Press, Oxford, United Kingdom, second edition edition, 2017.

5 S. Becker, H. M. Urbassek, M. T. Horsch, and H. Hasse. Contact angle of sessile drops in Lennard-Jones systems. *Langmuir*, 30(45):13606–13614, 2014. doi:10.1021/la503974z.

6 H. J. C. Berendsen, J. P. M. Postma, W. F. van Gunsteren, A. DiNola, and J. R. Haak. Molecular dynamics with coupling to an external bath. *The Journal of Chemical Physics*, 81(8):3684–3690, 1984. doi:10.1063/1.448118.

7 E. Brinksmeier, J. C. Aurich, E. Govekar, C. Heinzel, H.-W. Hoffmeister, F. Klocke, J. Peters, R. Rentsch, D. J. Stephenson, E. Uhlmann, K. Weinert, and M. Wittmann. Advances in modeling and simulation of grinding processes. *CIRP Annals*, 55(2):667–696, 2006. doi:10.1016/j.cirp.2006.10.003.

8 E. Brinksmeier, C. Heinzel, and M. Wittmann. Friction, cooling and lubrication in grinding. *CIRP Annals*, 48(2):581–598, 1999. doi:10.1016/S0007-8506(07)63236-3.

9 E. Brinksmeier, D. Meyer, A. G. Huesmann-Cordes, and C. Herrmann. Metalworking fluids–mechanisms and performance. *CIRP Annals*, 64(2):605–628, 2015. doi:10.1016/j.cirp.2015.05.003.

10 M. Bugel and G. Galliero. Thermal conductivity of the Lennard-Jones fluid: An empirical correlation. *Chemical Physics*, 352(1-3):249–257, 2008. doi:10.1016/j.chemphys.2008.06.013.

11 Y. H. Chen, H. Han, F. Z. Fang, and X. T. Hu. MD simulation of nanometric cutting of copper with and without water lubrication. *Science China Technological Sciences*, 57(6):1154–1159, 2014. doi:10.1007/s11431-014-5519-z.

12 F. Diewald, M. P. Lautenschlaeger, S. Stephan, K. Langenbach, C. Kuhn, S. Seckler, H.-J. Bungartz, H. Hasse, and R. Müller. Molecular dynamics and phase field simulations of droplets on surfaces with wettability gradient. *Computer Methods in Applied Mechanics and Engineering*, 361:112773, 2020. doi:10.1016/j.cma.2019.112773.

13 Y. Dong, Q. Li, and A. Martini. Molecular dynamics simulation of atomic friction: A review and guide. *Journal of Vacuum Science & Technology A: Vacuum, Surfaces, and Films*, 31(3):030801, 2013. doi:10.1116/1.4794357.

14 H. Edelsbrunner, D. Kirkpatrick, and R. Seidel. On the shape of a set of points in the plane. *IEEE Transactions on Information Theory*, 29(4):551–559, 1983. doi:10.1109/TIT.1983.1056714.

15 J. P. Ewen, D. M. Heyes, and D. Dini. Advances in nonequilibrium molecular dynamics simulations of lubricants and additives. *Friction*, 6(4):349–386, 2018. doi:10.1007/s40544-018-0207-9.

16 Y. Gao, A. Brodyanski, M. Kopnarski, and H. M. Urbassek. Nanoscratching of iron: A molecular dynamics study of the influence of surface orientation and scratching direction. *Computational Materials Science*, 103:77–89, 2015. doi:10.1016/j.commatsci.2015.03.011.

17 Y. Gao, C. J. Ruestes, D. R. Tramontina, and H. M. Urbassek. Comparative simulation study of the structure of the plastic zone produced by nanoindentation. *Journal of the Mechanics and Physics of Solids*, 75:58–75, 2015. doi:10.1016/j.jmps.2014.11.005.

18 Y. Gao and H. M. Urbassek. Evolution of plasticity in nanometric cutting of Fe single crystals. *Applied Surface Science*, 317:6–10, 2014. doi:10.1016/j.apsusc.2014.08.020.

19 Y. B. Guo, Y. C. Liang, M. J. Chen, Q. S. Bai, and L. H. Lu. Molecular dynamics simulations of thermal effects in nanometric cutting process. *Science China Technological Sciences*, 53(3):870–874, 2010. doi:10.1007/s11431-009-0243-9.

20 T. Halicioğlu and G. M. Pound. Calculation of potential energy parameters from crystalline state properties. *Physica Status Solidi (a)*, 30(2):619–623, 1975. doi:10.1002/pssa.2210300223.

21 M. Heier, S. Stephan, J. Liu, W. G. Chapman, H. Hasse, and K. Langenbach. Equation of state for the Lennard-Jones truncated and shifted fluid with a cut-off radius of 2.5 σ based on perturbation theory and its applications to interfacial thermodynamics. *Molecular Physics*, 116(15-16):2083–2094, 2018. doi:10.1080/00268976.2018.1447153.

22 C. Heinzel, B. Kirsch, D. Meyer, and J. Webster. Interactions of grinding tool and supplied fluid. *CIRP Annals*, 69(1):624–645, 2020. doi:10.1016/j.cirp.2020.05.001.

23 Y.-L. Huang, T. Merker, M. Heilig, H. Hasse, and J. Vrabec. Molecular modeling and simulation of vapor–liquid equilibria of ethylene oxide, ethylene glycol, and water as well as their binary mixtures. *Industrial & Engineering Chemistry Research*, 51(21):7428–7440, 2012. doi:10.1021/ie300248z.

24 B. Kirsch, S. Basten, H. Hasse, and J. C. Aurich. Sub-zero cooling: A novel strategy for high performance cutting. *CIRP Annals*, 67(1):95–98, 2018. doi:10.1016/j.cirp.2018.04.060.

25 F. Klocke. *Fertigungsverfahren 2: Zerspanung mit geometrisch unbestimmter Schneide*. VDI-Buch. Springer Berlin Heidelberg, Berlin, Heidelberg, 2017. doi:10.1007/978-3-662-53310-9.

26 M. P. Lautenschlaeger and H. Hasse. Transport properties of the Lennard-Jones truncated and shifted fluid from non-equilibrium molecular dynamics simulations. *Fluid Phase Equilibria*, 482:38–47, 2019. doi:10.1016/j.fluid.2018.10.019.

27 M. P. Lautenschlaeger, S. Stephan, M. T. Horsch, B. Kirsch, J. C. Aurich, and H. Hasse. Effects of lubrication on friction and heat transfer in machining processes on the nanoscale: A molecular dynamics approach. *Procedia CIRP*, 67:296–301, 2018. doi:10.1016/j.procir.2017.12.216.

28 M. P. Lautenschlaeger, S. Stephan, H. M. Urbassek, B. Kirsch, J. C. Aurich, M. T. Horsch, and H. Hasse. Effects of lubrication on the friction in nanometric machining processes: A molecular dynamics approach. *Applied Mechanics and Materials*, 869:85–93, 2017. doi:10.4028/www.scientific.net/AMM.869.85.

29 Y. Liu, B. Li, and L. Kong. A molecular dynamics investigation into nanoscale scratching mechanism of polycrystalline silicon carbide. *Computational Materials Science*, 148:76–86, 2018. doi:10.1016/j.commatsci.2018.02.038.

30 B. Magyar and B. Sauer. Methods for the simulation of the pressure, stress, and temperature distribution in the contact of fractal generated rough surfaces. *Proceedings of the Institution of Mechanical Engineers, Part J: Journal of Engineering Tribology*, 231(4):489–502, 2017. doi:10.1177/1350650115593962.

31 B. Meng, D. Yuan, and S. Xu. Study on strain rate and heat effect on the removal mechanism of SiC during nano-scratching process by molecular dynamics simulation. *International Journal of Mechanical Sciences*, 151:724–732, 2019. doi:10.1016/j.ijmecsci.2018.12.022.

32 A. Noreyan and J. G. Amar. Molecular dynamics simulations of nanoscratching of 3C SiC. *Wear*, 265(7):956–962, 2008. doi:10.1016/j.wear.2008.02.020.

33 S. Plimpton. Fast parallel algorithms for short-range molecular dynamics. *Journal of Computational Physics*, 117(1):1–19, 1995. doi:10.1006/jcph.1995.1039.

34 J. Ren, J. Zhao, Z. Dong, and P. Liu. Molecular dynamics study on the mechanism of AFM-based nanoscratching process with water-layer lubrication. *Applied Surface Science*, 346:84–98, 2015. doi:10.1016/j.apsusc.2015.03.177.

35 R. Rentsch and I. Inasaki. Effects of fluids on the surface generation in material removal processes –molecular dynamics simulation–. *CIRP Annals*, 55(1):601–604, 2006. doi:10.1016/S0007-8506(07)60492-2.

36 C. J. Ruestes, E. M. Bringa, Y. Gao, and H. M. Urbassek. Molecular dynamics modeling of nanoindentation. In *Applied nanoindentation in advanced materials*, pages 313–345. John Wiley & Sons, Ltd, 2017. doi:10.1002/9781119084501.ch14.

37 A. J. Schultz and D. A. Kofke. Comprehensive high-precision high-accuracy equation of state and coexistence properties for classical Lennard-Jones crystals and low-temperature fluid phases. *The Journal of Chemical Physics*, 149(20):204508, 2018. doi:10.1063/1.5053714.

38 S. Stephan, M. Dyga, H. M. Urbassek, and H. Hasse. The influence of lubrication and the solid–fluid interaction on thermodynamic properties in a nanoscopic scratching process. *Langmuir*, 35(51):16948–16960, 2019. doi:10.1021/acs.langmuir.9b01033.

39 S. Stephan, M. T. Horsch, J. Vrabec, and H. Hasse. MolMod – an open access database of force fields for molecular simulations of fluids. *Molecular Simulation*, 45(10):806–814, 2019. doi:10.1080/08927022.2019.1601191.

40 S. Stephan, M. P. Lautenschlaeger, I. A. Alhafez, M. T. Horsch, H. M. Urbassek, and H. Hasse. Molecular dynamics simulation study of mechanical effects of lubrication on a nanoscale contact process. *Tribology Letters*, 66(4):126, 2018. doi:10.1007/s11249-018-1076-0.

41 S. Stephan, M. Thol, J. Vrabec, and H. Hasse. Thermophysical properties of the Lennard-Jones fluid: Database and data assessment. *Journal of Chemical Information and Modeling*, 59(10):4248–4265, 2019. doi:10.1021/acs.jcim.9b00620.

42 I. Szlufarska, M. Chandross, and R. W. Carpick. Recent advances in single-asperity nanotribology. *Journal of Physics D: Applied Physics*, 41(12):123001, 2008. doi:10.1088/0022-3727/41/12/123001.

43 A. Travesset. Phase diagram of power law and Lennard-Jones systems: Crystal phases. *The Journal of Chemical Physics*, 141(16):164501, 2014. doi:10.1063/1.4898371.

44 K. V. Tretiakov and S. Scandolo. Thermal conductivity of solid argon from molecular dynamics simulations. *The Journal of Chemical Physics*, 120(8):3765–3769, 2004. doi:10.1063/1.1642611.

45 A. I. Vakis, V. A. Yastrebov, J. Scheibert, L. Nicola, D. Dini, C. Minfray, A. Almqvist, M. Paggi, S. Lee, G. Limbert, J. F. Molinari, G. Anciaux, R. Aghababaei, S. Echeverri Restrepo, A. Papangelo, A. Cammarata, P. Nicolini, C. Putignano, G. Carbone, S. Stupkiewicz, J. Lengiewicz, G. Costagliola, F. Bosia, R. Guarino, N. M. Pugno, M. H. Müser, and M. Ciavarella. Modeling and simulation in tribology across scales: An overview. *Tribology International*, 125:169–199, 2018. doi:10.1016/j.triboint.2018.02.005.

46 J. Vrabec, G. K. Kedia, G. Fuchs, and H. Hasse. Comprehensive study of the vapour–liquid coexistence of the truncated and shifted Lennard–Jones fluid including planar and spherical interface properties. *Molecular Physics*, 104(9):1509–1527, 2006. doi:10.1080/00268970600556774.

47 P. Wang, J. Yu, and Q. Zhang. Nano-cutting mechanical properties and microstructure evolution mechanism of amorphous/single crystal alloy interface. *Computational Materials Science*, 184:109915, 2020. doi:10.1016/j.commatsci.2020.109915.

48 J. Zhang, T. Sun, Y. Yan, and Y. Liang. Molecular dynamics study of scratching velocity dependency in AFM-based nanometric scratching process. *Materials Science and Engineering: A*, 505(1):65–69, 2009. doi:10.1016/j.msea.2008.10.049.

49 Z. Zhang, I. Alabd Alhafez, and H. M. Urbassek. Scratching an Al/Si interface: Molecular dynamics study of a composite material. *Tribology Letters*, 66(3):86, 2018. doi:10.1007/s11249-018-1038-6.

50 P.-Z. Zhu, C. Qiu, F.-Z. Fang, D.-D. Yuan, and X.-C. Shen. Molecular dynamics simulations of nanometric cutting mechanisms of amorphous alloy. *Applied Surface Science*, 317:432–442, 2014. doi:10.1016/j.apsusc.2014.08.031.